Computational Study of the Electronic and Structural Properties of Semiconductors with Chalcopyrite Structure

A. Habanyama[a,*], D. Silungwe[2], E. Phiri[2] and R. O. Manyala[2]
[1]*Department of Physics, Copperbelt University, Riverside, Kitwe, Zambia*
[2]*Department of Physics, University of Zambia, Lusaka, Zambia*

We use first-principle calculations based on the density functional theory to study some electronic properties of eight ternary semiconductors with the chalcopyrite structure. Both the local-density and the generalized gradient approximations are employed, which was done within the quantum-espresso software package. It was found that the local-density and the generalized gradient pseudo-potentials tended to under-estimate the size of the band gaps. A mean field Hubbard correction, *U* referred to as the Hubbard interaction parameter was added to the local-density energy functional as an attempt to make up for the deficiencies of the exchange-correlation energy in the local-density approximation. The method gave results that are close to the experimentally observed values. An empirical shift method was also employed. Our band structure calculations suggest that most chalcopyrite semiconductors have a direct gap. The k-vector position in the first Brillouin zone, at the minimum of the band gap, was found to be either near the L reciprocal lattice point or in the region between K and the center of the first Brillouin zone at Γ. The bulk modulus of each of the chalcopyrite materials was computed using Cohen's empirical formula [26]. It was found that the average error in our results of the bulk modulus for the chalcopyrites, where experimental results were available for comparison, was 6.3 %. $CuGaS_2$ is predicted as being the hardest of all the eight chalcopyrite materials investigated. Some impurity properties of the chalcopyrite semiconductors were also studied as well as energy of formation values were calculated for both vacant and dopant sites.

1. Introduction

Chalcopyrite-type semiconductors are ternary compounds with the tetragonal chalcopyrite crystal structure [1-3]. There are two types of chalcopyrite-type semiconductors, referred to as: $I - III - V\ I_2$ and $II - IV - V_2$, where the Roman numbers refer to the groups in the periodic table of the constituent elements. These two chalcopyrite types can be represented by the general formula, ABC_2 where, A could be Lithium (Li), Sodium (Na), Copper (Cu) or Silver (Ag) (from either group I or II), B could be Aluminium (Al), Gallium (Ga), Indium (In) or Titanium (Ti) (from either group III or IV) and C is Sulphur (S), Selenium (Se) or Tellurium (Te) (from either group V or VI).

Solar cells based on $I\text{-}III\text{-}VI_2$ and $II\text{-}IV\text{-}V_2$ chalcopyrite-type semiconductor materials have attracted considerable scientific interest due to their promising photovoltaic applications [4]. These semiconductors are attractive as absorber materials for photovoltaic devices due to their very high optical absorption coefficient for visible light ($\alpha \sim 10^4\ cm^{-1}$). One example is Copper-Indium-Sulphide ($CuInS_2$), which has an optical absorption coefficient greater than $10^5 cm^{-1}$ and a band gap of approximately 1.45eV, which matches the optimum value of 1.5eV, permitting a large absorption of the solar spectrum [5,6]. The high absorption makes these materials well suited for efficient conversion of solar light into electricity. Among all known thin film photovoltaic devices, solar cells based on these materials have reached the highest efficiencies [7,8].

Wide band gap chalcopyrite-type semiconductors have recently attracted the attention of several researchers [9]. A wide band gap semiconductor is an electronic material in which the energy of the valence-to-conduction band electronic transitions is approximately equal to 2eV [10]. Recently, the (Cu, Ag) GaX_2 chalcopyrite alloy system, with X being: S, Se or Te, has attracted a lot of attention because these materials have large direct band gaps between 1.68 and 2.65eV. This is the desirable band gap range for applications in high-efficiency tandem solar cells [11]. In these cells, most of the incoming photons with energies greater than 1.68eV are absorbed within the first micrometers of the chalcopyrite materials [11]. Another reason why chalcopyrite-type semiconductors have attracted a

---

[*] adrian.habanyama@cbu.ac.zm

lot of interest is because of their promising applications in nonlinear optics [12-14] and spintronics [15,16].

With recent progress in computational performance and strategy, computer simulations are increasingly used by theoretical physicists and physical chemists to understand properties of matter and make specific predictions for real materials and experimentally observable phenomena. This has been exploited by *ab initio* (first principles) simulation methods like the density functional theory (DFT) [17,18]. The advent of DFT and the invention of *ab initio* pseudo-potentials have made it possible to calculate, ground state electronic and structural properties, as well as to predict the stability of crystalline phases in solids.

In standard DFT calculations, there are two popular approximations for the exchange-correlation energy functional: the local density approximation (LDA) [19, 20] and the generalized gradient approximation (GGA) [21]. These standard DFT functionals sometimes do not provide good predictions, especially when they are applied to some transition-metal compounds like chalcopyrite semiconductors. A recent method aimed at correcting the limitations of standard DFT functionals for this class of materials is the DFT + Hubbard *U* (DFT+*U*) method. In the DFT+*U* method, the Coulomb interaction among electrons on a single transitional metal site is explicitly included in the total energy functional in a way similar to the *U*-term in the well-known Hubbard model. The DFT+*U* approach used in this work is the LDA+*U* method.

In a simplified version [22] of the rotationally invariant formulation [23] of the LDA + *U* method, the energy functional is expressed as

$$E_{LDA+U} = E_{LDA} + \sum_{I,\sigma} \frac{U^I}{2} Tr\left[n^{I\sigma}(1 - n^{I\sigma}\right] \qquad (1)$$

Where, $n^{I\sigma}$ are the atomic occupation matrices, which are projections of the Kohn-Sham [17] states on a set of localized orbitals. *U*, the Hubbard interaction parameter, represents the strength of the effective on-site Coulomb repulsion between electrons. The Hubbard *U* parameters adopted in this work were calculated using the linear response theory [24] as implemented in the quantum-espresso package [25].

In this work, we examine the ground-state electronic and structural properties of eight semiconductors with the chalcopyrite structure using first principles employing the quantum-espresso simulation package [25], which performs plane-wave pseudo-potential total energy calculations.

The bulk modulus of a material may be defined as the ratio of the change in pressure to the fractional volume compression. A way to compute the bulk modulus of a material is by using Cohen's empirical formula [26] given as

$$B = \frac{(1971 - 220\lambda)}{d^{3.5}} \qquad (2)$$

This expression has been found to be useful for zinc blende compounds [27]. In Cohen's formula λ is taken to be 1 and 2 for III-V and II-VI compounds respectively; the variation in the value of λ being as a consequence of the difference in ionicity. The *d* in the formula is the bond length. This formula is designed such that the value of *B* is in GPa, whereas *d* is in Å. A modified form of Eqn. (2), which can be used for chalcopyrites is

$$B = \frac{1971 - 220\lambda}{4} \sum_{i=1,2,3,4} \frac{1}{d_i^{3.5}} \qquad (3)$$

This form of the expression takes into account the fact that the bond lengths in chalcopyrites are not equal due to the two different types of cations.

The chalcopyrite compounds of chemical formula II-IV-V_2 and I-III-VI_2 can be thought of as being derived from a parent binary compound with formula, III-V and II-VI, respectively, by replacing the group-III element by alternating a group-II and group-IV element or the group-II by a group-I and group-III elements. The value of λ is therefore expected to be 1 and 2 for II-IV-V_2 and I-III-VI_2 compounds as in their parent binary analogues, the III-V and II-VI compounds, respectively.

It can be shown for the zinc blende and chalcopyrite structure that the average nearest neighbor distance is given by

$$d = \frac{\sqrt{3}}{4} a \qquad (4)$$

Where, a is the lattice constant. This result is used in this work to determine the average bulk modulus using Cohen's formula.

It is well known that the local density approximation often underestimates the band gap in strongly correlated systems. Jiang et al. [28] estimated empirical shift corrections to the LDA derived chalcopyrite band gaps based on the similarities of the band structures with the parent and grandparent compounds. The reason for the band gap underestimation by the LDA correlation functional for strongly correlated systems is that the Kohn-Sham one-particle equation [17] does not provide quasi-particle excitation energies. The equation for quasi-particle energies in the so-called GW method [29-31] differs from the Kohn-Sham equation by the fact that the local exchange-correlation potential is replaced by a nonlocal energy operator. Jiang et al. [28] adjusted the LDA band gaps so as to reproduce the GW results of Zakharov et al. [32] rather than experimental results because they wished to adjust not only the minimum gaps, as given by available experimental results, but both gaps at the center of the first Brillouin zone, Γ and at the reciprocal lattice point, X. They found that fairly good agreement with GW results could be obtained by applying a universal empirical shifts of either 0.14 Ry (1.905 eV) or 0.21Ry (2.858 eV) to the LDA results.

2. Crystal Structure

We refer to the chemical groups in Roman numerals as I, II, III, IV, V and VI. These correspond to the elements in the periodic table column numbers, 11, 12, 13, 14, 15 and 16, respectively. III-V semiconductors such as GaAs and InP have the zinc blende crystal structure possessed by ZnS and several other II-VI compounds. In the zinc blende structure, there are two inter-penetrating face centered cubic sub-lattices. One is occupied by the cations (from group III or II) and the other by anions (from group VI or V). In a ternary chalcopyrite the anion sub-lattice remains but the cation sub-lattice is filled by two types of cations, one of a high valence and another of a lower valence, which are arranged in an ordered manner. Since the cation sites are equally share by two atomic types it means that there are twice as many anion atoms as any single cation atom resulting in the chemical compositions, I −III − V I_2 and II − IV – V_2. We first present the valence electronic configurations of all the elements that constitute the materials studied in this work.

Group I → Cu (11 → $3d^{10}4s$) and Ag (11 → $4d^{10}5s$) Group II → Zn (12 → $3d^{10}4s^2$)	High valence cations
Group III → Ga (3 → $4s^2 4p$) and In (3 → $5s^2 5p$) Group IV → Si (4 → $3s^2 3p^2$) and Sn (4 → $5s^2 5p^2$)	Lower valence cations
Group V → As (5 → $4s^2 4p^3$) Group VI → S (6 → $3s^2 3p^4$), Se (6 → $4s^2 4p^4$) and Te (6 → $5s^2 5p^4$)	Anions

The transition metals Cu, Ag and Zn provide the high valence cations, the first number in the brackets gives the valence.

The chalcopyrites that were studied in this work are:

I – III – VI_2: $AgGaSe_2$, $AgGaS_2$, $AgGaTe_2$, $CuGaS_2$, $CuInS_2$, $CuInSe_2$

II – IV – V_2: $ZnSiAs_2$, $ZnSnAs_2$

The covalent bonding mechanisms in these crystals are facilitated by hybridization of the valence electronic states (outermost orbitals) by mixing them to form new orbitals like sp^3 hybrid orbitals which form the bonds.

The primitive cell of the zinc blende structure has only two atoms but the reduced symmetry due to the two kinds of cations in the chalcopyrite structure leads to a primitive cell of eight atoms. Compared to the face centered cubic Bravais cell of the zinc blende, the unit cell is doubled along the crystal *c* axis.

Each anion in the chalcopyrite structure is at the center of a tetrahedron with four cations at each corner. Since the anion is bonded to two types of cations, the respective bond lengths are not necessarily identical and therefore the tetrahedron is not regular. Usually the anions are closer to the cations of higher valence, this distorts the anion sublattice. It has been shown that such a shift of anions is a consequence of atomic sizes [33].

The chalcopyrite crystal structure has a body-centered tetragonal Bravais lattice. If we choose the primitive unit-cell lattice vectors as, $\boldsymbol{a} = (a/2)\boldsymbol{i} + (a/2)\boldsymbol{j} - (c/2)\boldsymbol{k}$, $\boldsymbol{b} = (a/2)\boldsymbol{i} - (a/2)\boldsymbol{j} + (c/2)\boldsymbol{k}$ and $\boldsymbol{c} = -(a/2)\boldsymbol{i} + (a/2)\boldsymbol{j} + (c/2)\boldsymbol{k}$, then the unit-cell atomic positions are:

Group I or II cations → $(0,0,0)$, $(a/2,0,c/4)$;

Group III or IV cations → $(a/2,a/2,0)$, $(0,a/2,c/4)$;

Group VI or V anions→ $(ua,a/4,c/8)$, $(-ua,-a/4,c/8)$, $(a/4,-ua,-c/8)$, $(-a/4,ua,-c/8)$

The distortion in the anion sub-lattice is represented by u, for the ideal structure $u = ¼$. For the ideal structure the ratio $\eta = (c/2a)$ is equal to one but in most cases $\eta < 1$ and $u > 1/4$. It can be seen from the atomic positions that there are eight atoms per primitive cell which is two formula units since the chalcopyrite formula has four atoms.

3. Computational Details

First-principles calculations were performed using the quantum-espresso *ab initio* simulation package [25] based on density functional theory [17,18]. The electronic exchange-correlation interactions are treated by the LDA in the scheme of Ceperley and Alder [19] as parameterized by Perdew and Zunger [20], and the GGA of Perdew, Burke and Ernzerhof [21]. The one-electron pseudo-orbitals are expanded over a plane wave basis set that includes all plane waves whose kinetic energy $\hbar^2k^2/2m < E_{\mathrm{cut}}$, where k is the wave vector, m the electron mass and E_{cut} the chosen cutoff energy. For all calculations reported in this work, the basis set contains plane waves up to an energy cutoff of 50 Ry. 6×6×6 Monkhorst-Pack [34] k-point mesh grids were used for sampling in the Brillouin zone. The chosen plane wave cutoff and the number of k-points allowed a convergence of the total energy to within 1 meV/atom.

The parameters a, η and u could be obtained by total energy minimization but this relaxation process was not adopted in this work because such a relaxation appeared to significantly affect the band structure, available experimental values [35, 36,37] of these structural parameters were used.

For a material with n vacancies, we used the following expression to determine the energy of formation E_f given as

$$E_f = E_{tot}[N-n;n] - \frac{N-n}{N} E_{tot}[N;0] \qquad (5)$$

For any material with n dopants the following expression was used:

$$E_f = E_{tot}[N;n] - E_{tot}[N;0] \qquad (6)$$

In the two expressions, N is the total number of atoms per unit cell while E_{tot} is the total energy per unit cell as determine by the quantum-espresso software. $E_{tot}[N;0]$ is the energy before the introduction of any defect, it is obtained after performing a self-consistent field (SCF) energy calculation on the material under investigation using the quantum-espresso software package. The $E_{tot}[N\text{-}n;n]$ is the total energy obtained from the SCF output file of a defect material with n vacancies per unit cell. This value is obtained after carrying out a relaxation operation on the unit cell structure, that is to say that the atomic positions were allowed to self-adjust according to the determined interatomic forces, until equilibrium of the system was achieved. The $E_{tot}[N;\ n]$ is the energy per unit cell of a doped material with n dopant atoms per unit cell and was also obtained from an SCF calculation coupled with a relaxation operation.

4. Results

Crystal structure diagrams were constructed for all the eight chalcopyrites using the crystalline structure visualization and analyzer software package, xcrysden [38]. The result for $AgGaS_2$ is presented in Fig. 1.

Electronic band structure calculations were carried out for the eight chalcopyrites, using both LDA and GGA functionals. Since the chalcopyrite structure is a derivative of the zinc blende structure, it is common to calculate the band structure of chalcopyrites in the zinc blende brillouin zone. This is the approach used in this work. The k-space path that we use in the first Brillouin zone of the zinc blende crystal structure is $\Gamma \to L \to \Gamma \to X \to W \to K \to \Gamma$.

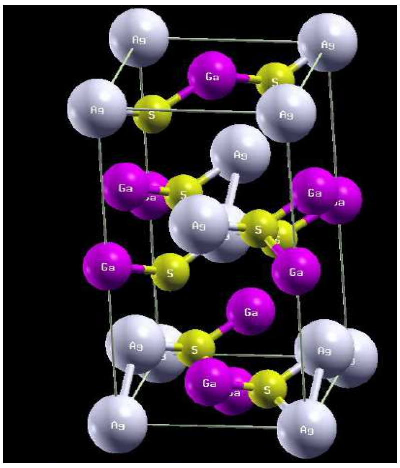

Fig.1: Chalcopyrite crystal structure of $AgGaS_2$, generated by xcrysden [38]

The band structures derived from the LDA and GGA functionals were similar, we therefore do not include a band structure diagrams for the GGA functional but summarize the GGA results in Table 1. We present some representative LDA and LDA+*U* results of both band structure and density of states in the diagrams of Fig. 2 and Fig. 3. The origin of the energy axis lies slightly above the Fermi level.

The band gap predicted by the LDA functional for $AgGaS_2$ in Figs. 2 (a) and (b) was effectively zero. Figs. 3 (a) and (b) obtained by the application of the LDA+*U* show an energy band gap of 1.2 eV. It is seen from both the band structure and density of states diagrams in Fig. 3 that the energy gap opens up between -1.0 eV and -2.0 eV when the LDA+*U* method is applied. It can be seen that the origin of the energy axis lies slightly above the Fermi level. This result was obtained by using a Hubbard *U* value of 5.0.

Table 1 gives a compilation of the results obtained using the LDA and GGA correlation functionals. Experimental values are included for comparison however two experimental values were not available.

It can be seen from Table 1 that both the LDA and GGA exchange correlation functionals greatly underestimate the values of the band gaps for ternary chalcopyrites.

The results of the LDA+*U* method are shown in Table 2. Jiang's upward empirical shift of 0.14 Ry was applied directly to the LDA derived values, these results are also shown in Table 2. Errors with reference to experimental values are included.

Table 1: LDA and GGA electronic band gap results

No.	Compound	*a*(Å)	*c*/*a*(Å)	*u*	E_g(LDA) (eV)	E_g(GGA) (eV)	Expt E_g (eV)
1.	$AgGaS_2$	5.74	1.78	0.309	0.00	0.00	2.70[39]
2.	$AgGaSe_2$	5.97	1.82	0.301	0.00	0.10	1.85[40]
3.	$AgGaTe_2$	6.28	1.895	0.277	0.15	0.25	1.3[41]
4.	$CuGaS_2$	5.347	1.953	0.262	0.00	0.00	1.67[42]
5.	$CuInS_2$	5.523	2.014	0.46	0.15	0.10	1.5[41]
6.	$CuInSe_2$	5.781	2.064	0.234	0.40	0.50	1.04[43]
7.	$ZnSiAs_2$	5.606	1.943	0.265	0.00	0.00	-
8.	$ZnSnAs_2$	5.852	2.00	0.250	0.00	0.00	-

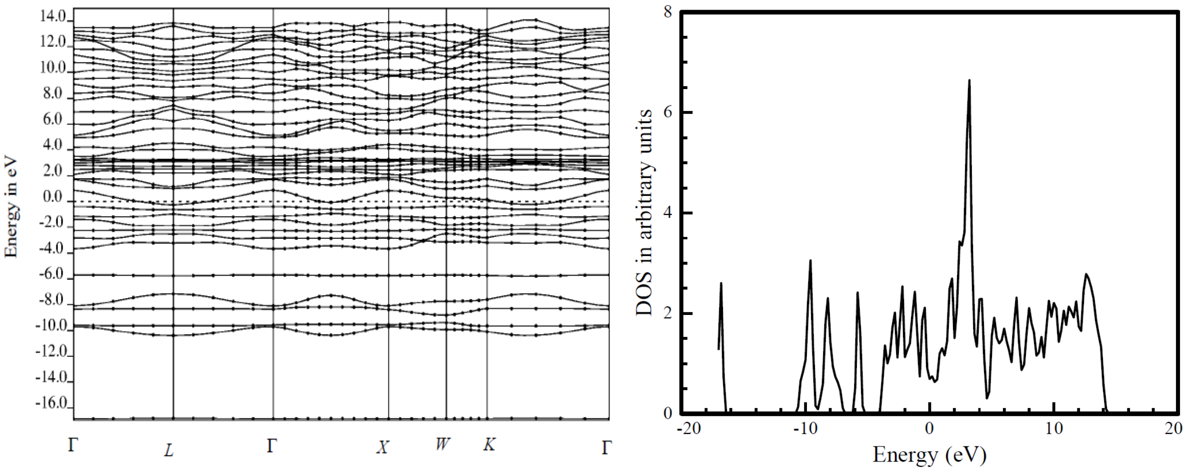

(a) (b)

Fig.2: (a) Band structure diagram for $AgGaS_2$ using the LDA functional. (b) Density of states diagram for $AgGaS_2$ using the LDA functional. The observed band gap is effectively zero

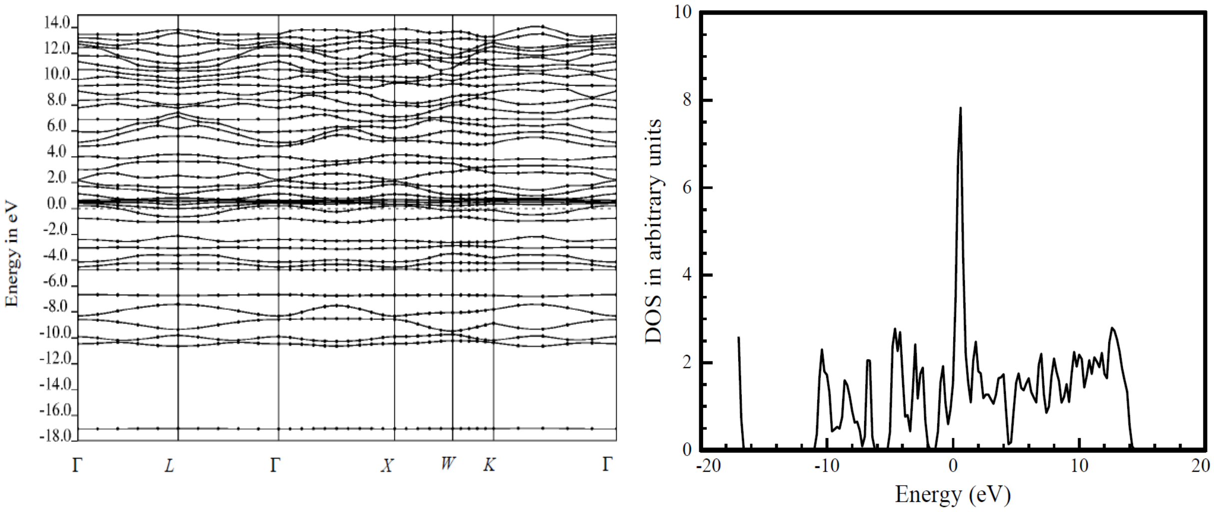

(a) (b)

Fig.3: (a) Band structure diagram for $AgGaS_2$ using the LDA+*U* method. (b) Density of states diagram for $AgGaS_2$ using the LDA+*U* method

Two results for the LDA+*U* method were inconclusive. The average error in the LDA+*U* method was 0.6eV while that in the empirical shift was 0.63eV.

Results obtained for the bulk modulus of the chalcopyrites investigated, using Cohen's formula for both λ = 1 and λ = 2, are shown in Table 3. Experimental values were not available for three of the materials in the table.

In Table 4 we have presented the value of *B* for either λ = 1 or λ = 2 depending on which λ gives a corresponding value of *B* which is closest to the experimental value for the material. Errors are included and cases where no experimental values are available are left blank.

Table 2: LDA+*U* and empirical shift electronic band gap results

Compound	LDA E_g (eV)	LDA+*U* E_g (eV)	Error in LDA+*U* (eV)	Empirically shifted E_g (eV)	Error in Empirical shift (eV)	Experimental value (eV)
$AgGaS_2$	0	1.2	1.5	1.9	0.8	2.70[39]
$AgGaSe_2$	0	1.2	0.7	1.9	0.1	1.85[40]
$AgGaTe_2$	0.15	1.2	0.1	2.1	0.8	1.3[41]
$CuGaS_2$	0.0	1.6	0.1	1.9	0.2	1.67[42]
$CuInS_2$	0.15	inconclusive	inconclusive	2.1	0.6	1.5[41]
$CuInSe_2$	0.4	inconclusive	inconclusive	2.3	1.3	1.04[43]
$ZnSiAs_2$	0.0	0.0	-	1.9	-	-
$ZnSnAs_2$	0.0	0.2	-	1.9	-	-

Table 3: Results obtained for the bulk modulus, investigated using Cohen's formula for both $\lambda = 1$ and $\lambda = 2$. Experimental values were not available for three of the materials

Compound	*a* (Å)	Average interatomic distance, *d* (Å)	Bulk modulus, *B* using $\lambda = 1$ (GPa)	Bulk modulus, *B* using $\lambda = 2$ (GPa)	Experimental bulk modulus, *B* (GPa)
$AgGaS_2$	5.74	2.486	72.3	63.2	77.6[44]
$AgGaSe_2$	5.97	2.585	63.1	55.1	54.8[44]
$AgGaTe_2$	6.28	2.719	52.8	46.2	38.9[45]
$CuGaS_2$	5.347	2.315	92.8	81.1	-
$CuInS_2$	5.523	2.392	82.7	72.3	75[46]
$CuInSe_2$	5.781	2.503	70.6	61.7	72[46]
$ZnSiAs_2$	5.606	2.428	78.5	68.7	-
$ZnSnAs_2$	5.852	2.534	67.6	59.1	-

Table 4: Error calculations, where experimental values were available, for the results obtained of the bulk modulus for the chalcopyrites investigated

Compound	Bulk modulus, *B* by Cohen's formula (GPa)	Experimental results of the bulk modulus, *B* (GPa)	Error in the Cohen method (GPa)	Percentage error in the Cohen method
$AgGaS_2$	72.3	77.6[44]	5.3	6.8
$AgGaSe_2$	55.1	54.8[44]	0.3	0.6
$AgGaTe_2$	46.2	38.9[45]	7.3	18.8
$CuGaS_2$	-	-	-	-
$CuInS_2$	72.3	75[46]	2.7	3.6
$CuInSe_2$	70.6	72[46]	1.4	1.9
$ZnSiAs_2$	-	-	-	-
$ZnSnAs_2$	-	-	-	-

Impurity properties of the chalcopyrites were investigated. Our method was first tested for silicon. We determined the energy of formation of a single Si vacancy per unit cell at the position, (0.25, 0.25, 0.25). The value obtained was 3.33eV per unit cell, this is in agreement with experimentally obtained values which are reported to be between 3.17eV [21] and 3.6eV [47].

Energy of formation of Cu vacancies and silver impurities at four (0.50, 0.00, 0.25) positions per unit cell in $CuInSe_2$ was calculated. The crystal structures of the $CuInSe_2$, $CuInSe_2$ with vacancy defects and $CuInSe_2$ with Ag dopant impurities, as generated using the xcrysden software, are shown in Fig. 4.

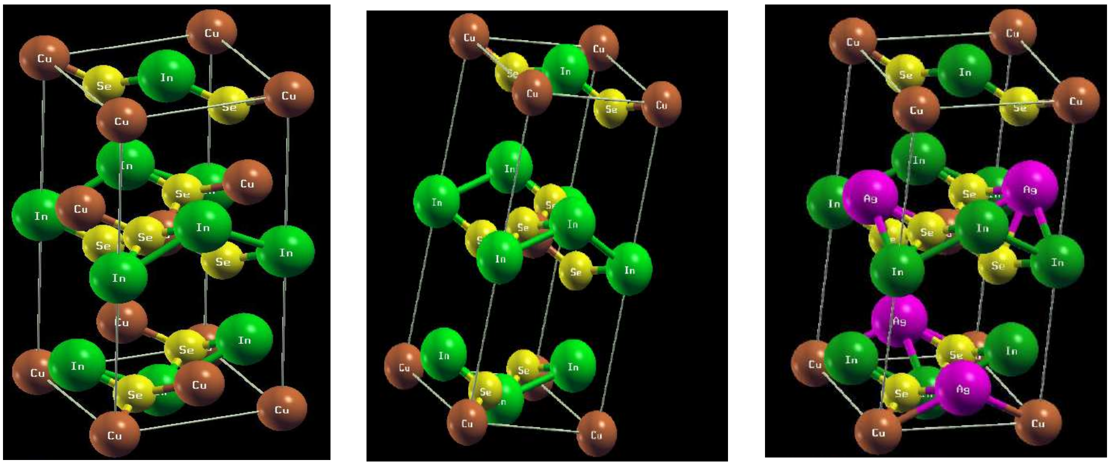

(a) (b) (c)

Fig.4: (a) Crystal structure of $CuInSe_2$. (b) $CuInSe_2$ with Cu vacancies at four (0.50, 0.00, 0.25) positions. (c) Silver impurities at four (0.50, 0.00, 0.25) positions in $CuInSe_2$

Similar calculations as those carried out for $CuInSe_2$ were carried out for the other chalcopyrites. Energy of formation results for vacancy defects at four (0.50, 0.00, 0.25) positions per unit cell are presented in Table 5.

Table 5: Energy of formation per unit cell for chalcopyrites with vacancy defects at four (0.50, 0.00, 0.25) positions

Chalcopyrite (4 vacancies)	Our E_f Results (eV)
$AgGaS_2$	-47.82 Ry
$AgGaSe_2$	-46.745Ry
$CuGaS_2$	-47.045Ry
$CuInS_2$	-75.435Ry
$CuInSe_2$	-72.88Ry
$ZnSiAs_2$	-35.34Ry
$ZnSnAs_2$	-59.284Ry

Energy of formation results for selected dopant defects at four (0.50, 0.00, 0.25) positions per unit cell are presented in Table 6.

Table 6: Energy of formation per unit cell for chalcopyrites with selected dopant defects at four (0.50, 0.00, 0.25) positions

Chalcopyrite (Doped)	Dopant	Our E_f Results (eV)
$AgGaS_2$	Li	67.00Ry
$AgGaSe_2$	Cu	-23.649Ry
$CuGaS_2$	Li	87.01Ry
$CuInS_2$	Ag	14.28Ry
$CuInSe_2$	Ag	13.56Ry
$ZnSiAs_2$	Be	103.42Ry
$ZnSnAs_2$	Be	54.012Ry

5. Discussion and Conclusion

Band structure calculations were carried out using LDA and GGA functionals but the results from these two exchange correlation functionals underestimated the values of the band gaps for chalcopyrites. More investigation was carried out using the LDA+U and the empirical shift methods. The LDA+U and empirical shift methods both gave results that were much closer to the results obtained experimentally. The two methods resulted in a similar average error in the band gap energy of 0.6eV.

Our band structure calculations suggest that most chalcopyrite semiconductors have a direct gap. The k-vector position in the first Brillouin zone at the minimum of the band gap was found to be either near the L reciprocal lattice point or in the region between K and the center of the first Brillouin zone at Γ.

It was mentioned in our introduction that λ was expected to take the values of 1 and 2 for chalcopyrites of type I-III-VI_2 and II-IV-V_2, respectively. However, a comparison of our results with experimental results shows that there are a few exceptions to this rule.

Table 7 lists the types of chalcopyrites, together with the value ofλ, which gives a corresponding value of B that is closest to the experimental value. A blank is left in cases where no experimental value is available.

We see that the bulk modulus values for $AgGaSe_2$, $AgGaTe_2$ and $CuInSe_2$ are better determined using $\lambda = 2$ rather than $\lambda = 1$, despite these chalcopyrites being of the type I-III-VI_2. We see from Table 4 that the average error in our results of the bulk modulus is 6.3 %.

Our theoretical predictions for the bulk modulus values of the three chalcopyrite materials, where no experimental results were available, are given in Table 8. These predictions were made using Table 3.

We see from Table 8 that $CuGaS_2$ is predicted as being the hardest of the eight chalcopyrite materials investigated.

Results obtained from our investigation of some impurity properties of the chalcopyrites show that the energy of formation for four vacancy defects per unit cell in the chalcopyrites lies between -75.435 Ry and -35.34 Ry. This predicts that the vacancies would be formed through exothermic processes. The energy of formation for four impurities per unit cell, of selected dopants, in the chalcopyrites investigated lies between 103.42Ry and -23.649Ry. All these results, except those for $AgGaSe_2$ doped with Cu, predict endothermic processes.

Acknowledgements

The authors would like to thank the Solar Energy Materials Project, in the Department of Physics at the University of Zambia for their financial support. We also thank the University of Swaziland for the use of their facilities.

Table 7: Results obtained for the bulk modulus of the chalcopyrites investigated, using Cohen's formula. This table picks the value of λ, which gives a corresponding value of B which is closest to the experimental value. A blank is left in cases where no experimental value is available

Compound	Type of compound	Theoretical bulk modulus, B (GPa)	Experimental bulk modulus B (GPa)	Optimum value of λ used
$AgGaS_2$	I-III-VI_2	72.3	77.6[44]	1
$AgGaSe_2$	I-III-VI_2	55.1	54.8[44]	2
$AgGaTe_2$	I-III-VI_2	46.2	38.9[45]	2
$CuGaS_2$	I-III-VI_2	-	-	-
$CuInS_2$	I-III-VI_2	72.3	75[46]	2
$CuInSe_2$	I-III-VI_2	70.6	72[46]	1
$ZnSiAs_2$	II-IV-V_2	-	-	-
$ZnSnAs_2$	II-IV-V_2	-	-	-

Table 8: Theoretical predictions for the bulk modulus values for chalcopyrites where no experimental results were available

Compound	Type of compound	Predicted values of the bulk modulus in GPa
$CuGaS_2$	I-III-VI_2	Close to or within the range: 81.1 to 92.8
$ZnSiAs_2$	II-IV-V_2	Close to or within the range: 68.7 to 78.5
$ZnSnAs_2$	II-IV-V_2	Close to or within the range: 59.1 to 67.6

References

[1] R. Bendorius, V. D. Prochukhan and A. Sileika, Phys. Stat. Sol. (b) **53**, 745 (1972).

[2] F. Chiker, B. Abbar, A. Tadjer, H. Aourag and B. Khelifa, Mat. Sci. & Eng. B **98**, 81 (2003).

[3] F. Chiker, B. Abbar, B. Bouhafs and P. Ruterana, Phys. Stat. Sol. (b), **241**, 305 (2004).

[4] S. E. Habas, H. A. S. Platt, M. F. A. M. van Hest and D. S. Ginley, Chem. Rev. **110**, 6571 (2010).

[5] S. Bandyopadhyaya, S. Chaudhuri and A. K. Pal, Solar Energy Materials & Solar Cells **60**, 323 (2000).

[6] J. Klaer, J. Bruns, R. Henninger, K. Siemer, R. Klenk, K. Ellmer and D. Bräunig, Semicond. Sci. Technol. **13**, 1456 (1998).

[7] A. Continenza, S. Massida, A. J. Freeman, T. M. De Pascale, F. Melonia and M. Serra, Phys. Rev. B **46**, 10070 (1992).

[8] A. G. Petukhov, W. R. L. Lambrecht and B. Segall, Phys. Rev. B **49**, 4549 (1993).

[9] S. Siebentritt, Thin Solid Films **403**, 1 (2002).

[10] V. S. Vavilov, Physics – Uspekhi, **37**, 269 (1994).

[11] T. J. Coutts, K. A. Emery and J. S. Ward, Prog. Photovoltaics **10**, 195 (2002).

[12] G. A. Verozubova et al., J. Crystal Growth, **213**, 334 (2000).

[13] L. Bai, Z. Lin, Z. Wang and C. Chen, J. Chem. Phys. **120**, 8772 (2004).

[14] L. Isaenkoet al., Crystal Growth & Design **5**, 1325 (2005).

[15] S. J. Pearton et al., Mater. Sci. and Eng. **R40**, 137 (2003).

[16] I. Zutic, J. Fabian and S. C. Erwin, IBM J. Res. & Dev. **50**, 121 (2006).

[17] W. Kohn and L. J. Sham, Phys. Rev. **140**, A1133 (1965).

[18] P. Hohenberg and W. Kohn, Phys. Rev. **136**, B864 (1964).

[19] D. M. Ceperley and B. J. Alder, Phys. Rev. Lett. **45**, 566 (1980).

[20] J. P. Perdew and A. Zunger, Phys. Rev. B **23**, 5048 (1981).

[21] J. P. Perdew, K. Burke and M. Ernezerhof, Phys. Rev. Lett. **77**, 3865 (1996).

[22] S. I. Dudarev, G. A. Botton, S. Y. Savrasov C. J. Humphreys and A. P. Sutton, Phys. Rev. B **57**, 1505 (1998).

[23] A. I. Liechtenstein, V. I. Anisimov and J. Zaanen, Phys. Rev. B **52**, R5467 (1995).

[24] M. Cococcioni and S. de Gironcoli, Phys. Rev. B **71**, 035105 (2005).

[25] P. Giannozzi, S. Baroni, N. Bonini, M. Calandra, R. Car, C. Cavazzoni, D. Ceresoli, G. I. Chiarotti, M. Cococcioni, I. Dabo, A. Dal Corso, S. De Gironcoli, S. Fabris, G. Fratesi, R. Gebauer, U. Gerstmann, C. Gougoussis, A. Kokalj, M. Lazzeri, I. Martin-Samos, N. Marzari, F. Mauri, R. Mazzarello, S. Paolini, A. Pasquarello, I. Paulatto, C. Sbraccia, S. Scandolo, G. Sclauzero, A. P. Seitsonen, A. Smogunov, P. Umari and R. M. Wentzcovitch, J. Phys.: Condens. Matter **21**, 395502 (2009).

[26] M. L. Cohen, Phys. Rev. B **3**, 7988 (1985).

[27] S. Mishra, “Structural, Electronic and Optical Properties of Chalcopyrite Type Semiconductors”, National Institute of Technology, Rourkela (2012).

[28] X. Jiang and Walter R. L. Lambrecht, Phys. Rev. B **69**, 035201 (2004).

[29] M. S. Hybertsen and S. G. Louie, Phys. Rev. B **34**, 5390 (1986).

[30] R. W. Godby, M. Schlüter and L. J. Sham, Phys. Rev. B **37**, 10159 (1988).

[31] F. Aryasetiawan and O. Gunnarsson, Rep. Prog. Phys. **61**, 237 (1998).

[32] O. Zakharov, A. Rubio, X. Blase, M. L. Cohen and S. G. Lourie, Phys. Rev. B **50**, 10780 (1994).

[33] J. E. Jaffe and A. Zunger, Phys. Rev. B **30**, 741 (1984).

[34] H. J. Monkhorst and J. D. Pack, Phys. Rev. B **13**, 5188 (1976).

[35] J. L. Shay and J. H. Wernick, *Ternary Chalcopyrite Semiconductors: Growth, Electronic Properties and Applications* (Pergamon Press, Oxford, New York, 1975).

[36] R. W. G. Wyckoff, *Crystal Structures* (Inter-science Publishers, New York, 1963).

[37] A. MacKinnon, Landolt-Börnstein, *Numerical Data and Functional Relationships in Science and Technology*, New Series (Springer, Berlin, Heidelberg, 1985).

[38] A. Kokalj, Comp. Mater. Sci. **28**, 155 (2003).

[39] S. Kobayashi, T. Ohno, N. Tsuboi, F. Kaneto and T. Maruyama, Jpn. J. Appl. Phys. **28**, 189 (1989).

[40] J. Shay, B. Tell, H. Kasper and L. Schiavone, Phys. Rev. B **5**, 5003 (1972).

[41] B. Tell, J. Shay and H. Kasper, Phys. Rev. B **9**, 5203 (1974).

[42] H. H. N. Yamamoto and T. Miyauchi, Jpn. J. Appl. Phys. **17**, 521 (1978).

[43] J. Shay, B. Tell, H. Kasper and L. Schiavone, Phys. Rev. B **7**, 4485 (1973).

[44] A. K. Arora and T. Sakuntala, J. Phys. Chem. Solids **54**, 381 (1993).

[45] R. Asokamamani, R. M. Amirthakumari, R. Rita and C. Ravi, Phys. Stat. Sol. (b) **213**, 349 (1999).

[46] T. Tinoco, A. Polian, D. Gomez and J. P Itie, Physica Status Solid **198**, 433 (1996).

[47] J. P. Perdew, K. Burke and M. Ernezerhof, Phys. Rev. **78**, 1396 (1997).

Received: 5 May, 2015
Accepted: 29 October, 2015